Geophys. J. Int. (1990) **103**, 25–31

Standard electrical conductivity of isotropic, homogeneous olivine in the temperature range 1200°–1500 °C

T. J. Shankland[1] and A. G. Duba[2]

[1]*Geophysics Group, MS D447, Los Alamos National Laboratory, Los Alamos, New Mexico 87545, USA*
[2]*Experimental Geophysics Group, MS L201, Lawrence Livermore National Laboratory, Livermore, California 94550, USA*

Accepted 1990 April 5. Received 1990 April 5; in original form 1988 March 17

SUMMARY

In order to produce electrical conductivity–temperature plots suitable for interpreting mantle conductivity profiles, we have used several spatial averaging schemes to reduce the orthorhombic conductivity tensor of olivine to that appropriate for an isotropic material. The starting data were new measurements of electrical conductivity σ in the three orthogonal principal directions of a San Carlos olivine (fayalite 9 per cent) to 1500 °C at 1 atmosphere total pressure. These measurements were made in a CO_2/CO atmosphere that provided an oxygen partial pressure of 10^{-4} Pa (10^{-9} atmosphere) at 1200 °C; this is slightly more reducing than the quartz–fayalite–magnetite (QFM) buffer curve. The highest [001] and lowest [010] conducting directions differ by a factor of 2.3. The next step was to obtain series and parallel bounds from the three principal directions; these absolute upper and lower bounds differ by 15 per cent. A standard conductivity curve comes from applying to the series and parallel curves various averaging schemes such as the Hashin–Shtrikman and Maxwell–Waff bounds or the effective medium, geometric mean, or (a new technique) self-similar methods; these all agree to within 3 per cent. The self-similar calculation demonstrates that the VRH method is a form of parallel average that is biased toward high values. The standard curve SO1 is given by $\sigma = 46.9 \exp(-1.38/kT) + 5.22 \times 10^8 \exp(-3.90/kT)$ where T is absolute temperature, k is the Boltzmann constant, and the activation energy is in eV. It is valid for the measurement interval of 1200°–1500 °C and can be used for extrapolation on either side of this range. Uncertainties associated with applying SO1 to inferring mantle temperatures are discussed.

Key words: electrical conductivity, geotherms, mantle temperature, olivine, spatial averaging schemes.

1 INTRODUCTION

A principal motivation for understanding electrical conductivity of minerals has been to use the strong temperature dependence of electrical conductivity for the purpose of inferring temperatures in the Earth from conductivity profiles (e.g., Hughes 1955; Runcorn & Tozer 1955; Tozer 1959). This approach is best suited to the lithosphere above and somewhat below the mantle high-conductivity layer (HCL) where the volumetric abundance of olivine is predominant. We parenthetically note that we do not consider the results in this paper to apply to the mantle HCL. In the HCL conductivities greater than 0.01–0.1 S m^{-1} have led to other hypotheses in which the relatively insulating silicate matrix is shunted by a higher conductivity, interconnected phase such as partial melt or fluid (summarized by Shankland *et al.* 1981) or elemental carbon (Duba & Shankland 1982). However, in calculating possible effects of these exceptional phases it is also useful to have an appropriate mean value for conductivity of the olivine matrix, e.g., as applied by Shankland & Waff (1977).

Although the electrical conductivity of an olivine single crystal has been measured under controlled oxygen fugacity to temperatures as high as 1660 °C (Duba, Heard & Schock 1974), there has previously been no determination of the complete conductivity tensor for a mantle olivine at controlled oxygen fugacity. Such data are required in order to calculate the average conductivity for an isotropic distribution of olivine that might occur at depth in the mantle or to investigate the possible extent of anisotropy. In

this paper we use the conductivity measured to 1500 °C on oriented single crystals from San Carlos, Arizona (9 per cent fayalite) to calculate an average conductivity appropriate for an isotropic, homogeneous aggregate. The data used here are selected from a fuller set of measurements of thermoelectric effect and electrical conductivity in forsterite and olivine as functions of temperature, oxygen fugacity fO_2, and crystallographic orientation (Schock, Duba & Shankland 1989).

2 EXPERIMENTAL PROCEDURE

Rectangular parallelepipeds were cut from a single crystal of San Carlos olivine, $(Mg_{0.91}, Fe_{0.09})_2\ SiO_4$ (Schock *et al.* 1989). The shortest dimension of each sample was within 1°–2° of a given crystallographic axis as determined by the Laue back-reflection method. The convention that we use for denoting crystallographic orientation in the orthorhombic crystal structure is space group Pbnm in which $a < c < b$. Sample thicknesses varied from 0.3 to 0.5 mm, and length and width varied from 3 to 7 mm. Iridium-foil electrodes (0.05 mm thick) were held in contact with the sample faces by a small compression spring located in the water-cooled portion of the experimental assembly (Duba & Nicholls 1973; Netherton & Duba 1978). This spring pushed on an alumina tube that contains the Pt–Pt/10 per cent Rh thermocouple assembly consisting of 0.5 mm wires welded to a 0.25 mm Pt foil. The sample-electrode sandwich was then held in contact with a similar thermocouple assembly that had no compression spring. An outer alumina tube served as the reaction frame. With this assembly it was possible to measure temperature on either side of the sample with a precision of at least ±1 °C; the thermocouples had been checked against the melting point of gold and agreed to ±2 °C. In addition, the platinum legs of the thermocouple served as leads for measurement of conductance by an impedance bridge operating at 1 kHz. Accuracy of the bridge was verified by standard resistors to be 1 per cent.

Oxygen fugacity for the data reported here was buffered by a mixture of CO_2:CO of 10:1, and the fugacity of the mix was checked by a calcia-doped zirconia sensor located in a separate furnace in order to avoid potential contamination by material outgassing from ceramics in the oxygen fugacity measuring assembly. This mixture yields an oxygen fugacity that is slightly more reducing than the quartz–fayalite–magnetite (QFM) buffer and produces an oxygen fugacity of about 10^{-4} Pa at 1200 °C. The fO_2–T trajectory of this 10:1 mixture is near the centre of the olivine stability field as depicted by Nitsan (1974). More importantly, at this fO_2 the sample can be heated to 1500 °C without partial melting of the fayalite component of olivine, as can be seen in fig. 1 of Nitsan (1974).

In a representative run such as Fig. 1(a) σ was measured as temperature was increased at the rate of 1 °C per minute to 1200 °C. After an equilibration time of at least 12 hr at 1200 °C, σ was measured on heating the sample to a temperature near 1500 °C and on cooling back to 1200 °C after an equilibration time of about 1 hr at the highest temperature. Several features of Fig. 1(a) are of interest. There is a high conductivity on initial heating to around 700 °C that has been attributed to the presence of alteration products at surfaces and dislocations—most likely magnetite (Duba & Nicholls 1973) which is known to decorate dislocations in olivine (Kohlstedt *et al.* 1976). Recent measurements (Duba, Young & Shankland 1988; Constable & Duba 1990), however, suggest that there could be substantial carbon deposition on the sample and within the furnace as the sample is heated through an initial low-fugacity range given by the CO_2:CO mix. In any case, we believe that the decrease in σ at temperatures above 700 °C was due to the loss of this surface phase as a result of the experimental conditions. This effect is not seen in all samples. In fact, this sample was the only one of the samples cut from the same crystal that showed this feature. Equilibration at 1200 °C resulted in a further slight decrease in conductivity. As the sample was heated, the oxygen fugacity of the experimental atmosphere increased and, for a constant gas mix, the fO_2–T trajectory was approximately parallel to the boundaries of the olivine stability field (Duba 1976).

Conductivity of a sample of the size used in this study requires about 2 hr to come to equilibrium after a change in oxygen fugacity at 1200 °C (Schock *et al.* 1989). Thus, data collected at a heating rate of 1 °C per minute would be slightly out of equilibrium because fO_2 of the gas mixture changes as temperature changes, and the sample requires time to adjust to the different conditions. However, because temperature enhances kinetic processes, data at 1500 °C approached equilibrium more rapidly. This statement is supported by the very small difference in values of σ upon heating and cooling between 1400° and 1500 °C compared with those between 1200° and 1300 °C in Fig. 1(b). The maximum difference in σ at any temperature is less than 0.1 $\log_{10}$ units and is insignificant for the purposes of this paper. Data were collected on heating from 1200 °C to the highest temperature for [100] and [010] and on cooling for [001].

3 DATA ANALYSIS

3.1 Curve fitting procedure

Before performing spatial averaging it was necessary to have the three components of conductivity on the same grid of points along the reciprocal temperature axis. It is then possible to obtain averages at each temperature point.

Electrical conductivity is the sum of several thermally activated processes described by exponential curves $\sigma_0 e^{-A/kT}$ where T is absolute temperature, k is the Boltzmann constant, and the activation energy A is in eV. The strong temperature dependence means that one conduction process usually dominates at a given temperature. However, because of indications that two conduction mechanisms operate in the temperature range 1200°–1500 °C (Schock *et al.* 1989) we used two such functions to fit the data. As in Constable & Duba (1990) we performed the non-linear fit with the Levenberg–Marquardt iterative method (Press *et al.* 1986). In this calculation the iterations were stopped when consecutive values of χ^2 agreed to one part in 10^5. Fig. 2 displays the experimental conductivities, the two exponential fits, and the best-fitting line that is the sum of the two exponential segments in each crystallographic direction. Table 1 gives values of the fitting

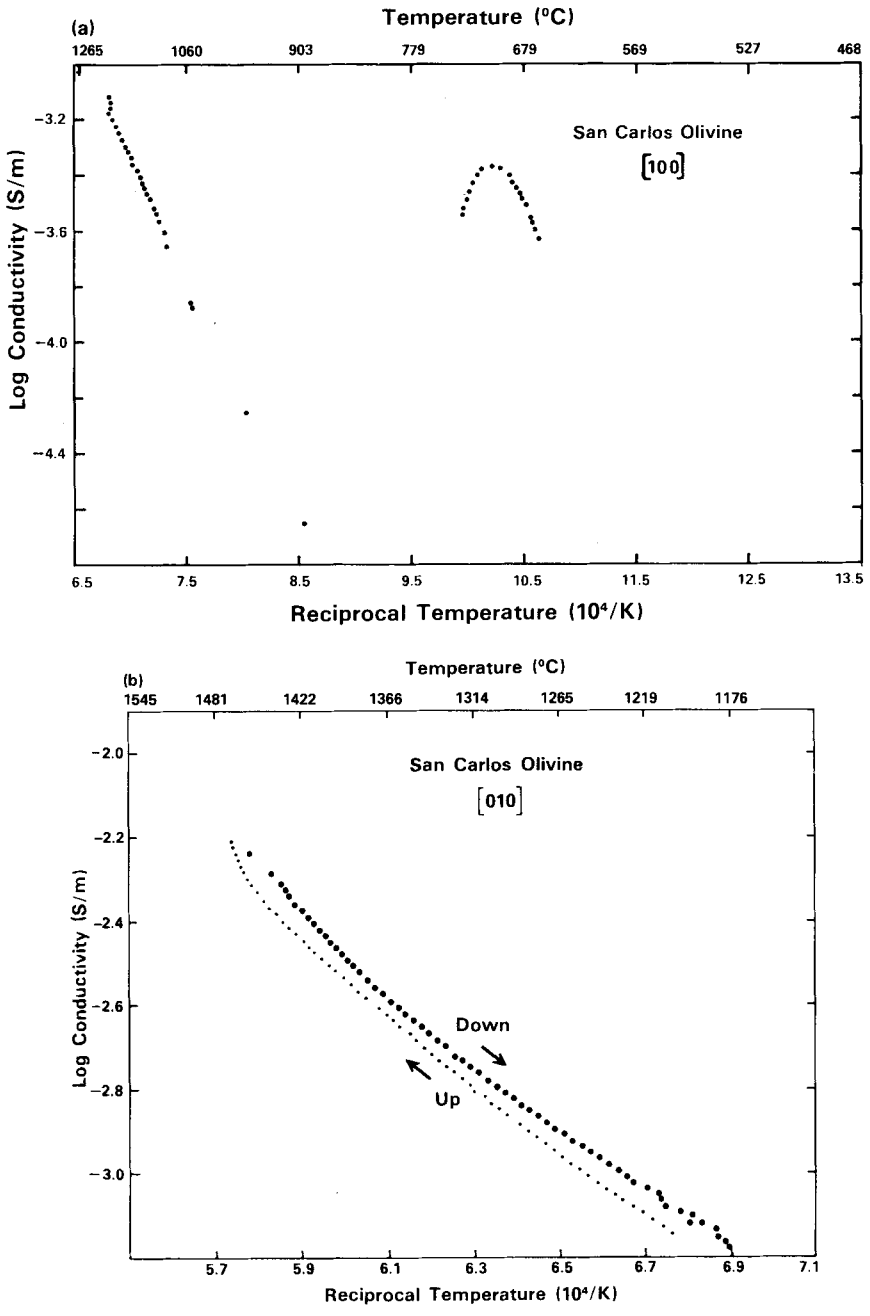

Figure 1. (a) Electrical conductivity of olivine on first heating from room temperature; the low-temperature peak does not reappear on subsequent reheating (see text). (b) Illustration of reproducibility of conductivity of olivine along [010] on heating and cooling.

parameters. Listed uncertainties are the square roots of the diagonal elements of the covariance matrix for the fitted parameters on the assumption of 1 per cent random error in measured conductivities. Systematic errors such as re-equilibration to changing fO_2 during temperature cycling were not included. In the case of [010] the very high activation energy, greater than the band gap of olivine, for the high-temperature segment probably results from the small number of data points in this range; we believe that it should be regarded merely as a fitting parameter and not assigned a physical significance.

Displaying the fits as in Fig. 2 has some advantages. First, the exponential functions are more likely to be physically significant (excepting the [010] case above) and are therefore more suitable for interpretation and extrapolation. Second, the fit is consequently likely to be better than, say, a power-law fit as previously attempted (Shankland & Duba 1987). Third, these fits demonstrate a useful check: the intersection point of the straight-line segments where the two segments have equal values must lie below the fitted line by a factor of 2 or by 0.3 on a $\log_{10}$ plot. Nearly all previous fits to conductivity, diffusion, or other activated processes have not met this readily visible criterion when more than one exponential was invoked. When they do not meet this criterion, the inferred activation energies are likely to be in error.

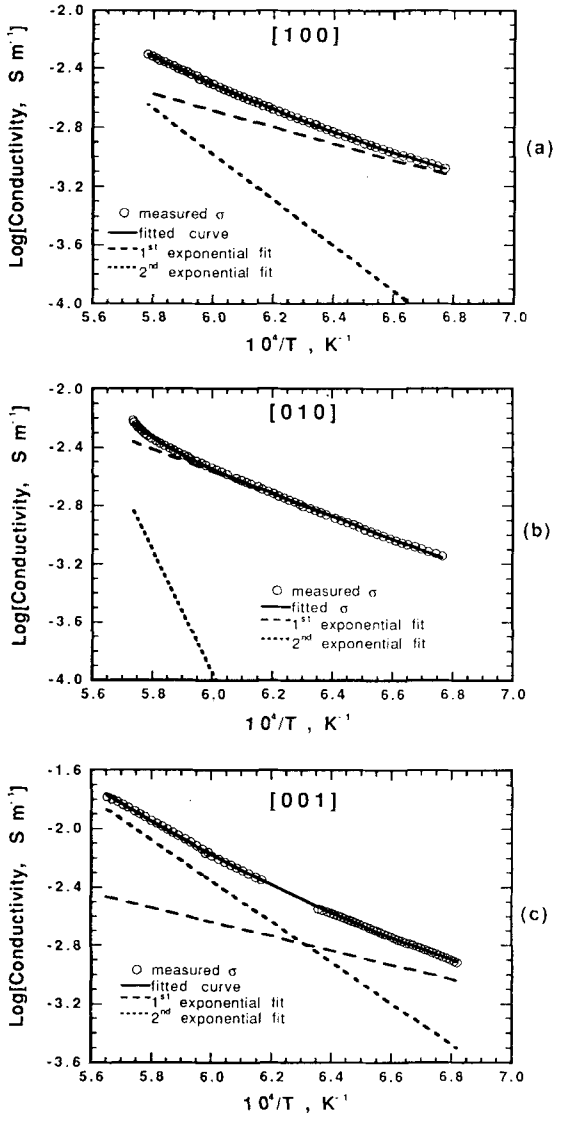

Figure 2. Measured data points of electrical conductivities along the principal directions of olivine. (a): [100], (b): [010], and (c): [001]. Long-dashed lines are the low-temperature exponential fits and short-dashed lines the high-temperature fits; their sum, the solid lines, are the best-fitting curves to the measured values. The straight lines intersect at a value log 2 = 0.3 below the fitted curve.

3.2 Averaging schemes

In order to use laboratory data to place bounds on mantle temperatures, it is necessary to take account of mineral textures. As a first approximation to an appropriate mantle material we consider the possible conductivity ranges of a principally olivine composition because of its volumetric dominance. We ignore contributions from phases of either lower conductivity such as pyroxene (Duba, Boland & Ringwood 1973) or much lower volume fraction such as spinel or garnet. A rock composed wholly of olivine grains could have its conductivity somewhere within the experimental curves of Fig. 2 depending on the degree of anisotropy. A heterogeneous, anisotropic rock composed of mineral grains in preferred orientations (as has been proposed for oceanic lithosphere formed at spreading ridges) would have components of its conductivity tensor bounded by the three principal (diagonal) values of the orthorhombic olivine conductivity tensor. For example, at 1394 °C ($10^4/T = 6$) the largest and smallest components differ by a factor of 2.3.

In the absence of information on texture it is useful to consider possible conductivities for an isotropic and homogeneous material in which all three orientations are present in equal volumes. We do this in more detail than is required by any geophysical application in order to demonstrate the degree of agreement, to allay contentions that one averaging scheme yields significantly better results, and to illustrate the methods. As the starting values for the spatial averages we used the set of three conductivities along the three major crystallographic axes. If we neglect grain boundary effects or porosity, the maximum and minimum conductivity values are the parallel and series solutions (e.g., Schulgasser 1976, 1977)

$$\sigma_p = (\sigma_a + \sigma_b + \sigma_c)/3, \tag{1a}$$

$$\sigma_s^{-1} = (\sigma_a^{-1} + \sigma_b^{-1} + \sigma_c^{-1})/3. \tag{1b}$$

Here σ_a, σ_b, and σ_c are the principal components of an orthorhombic conductivity tensor; in the case of olivine they are the conductivities along the crystallographic directions [100], [010], and [001]. Equations (1) are the Voight (1928) and Reuss (1929) averages, respectively. At 1394 °C, σ_p is only 15 per cent larger than σ_s showing that the restriction to homogeneity and isotropy is a strong constraint. The parallel and series bounds shown in Fig. 3 are narrow

Table 1. Coefficients of the expansion $\sigma = \sigma_1 e^{-A_1/kT} + \sigma_2 e^{-A_2/kT}$

Direction	$\log_{10}(\sigma_1$, S/m)	A_1, eV	$\log_{10}(\sigma_2$, S/m)	A_2, eV
[100]	0.66 ± .34	1.11 ± 0.10	6.3 ± 0.9	3.08 ± 0.3
[010]	2.03 ± 0.05	1.52 ± 0.02	22.2 ± 1.8	8.6 ± 0.6
[001]	0.31 ± 0.40	0.97 ± 0.11	6.0± 0.3	2.77 ± 0.10
Standard Olivine				
SO1	1.67 ± 0.16	1.38 ± 0.04	8.7 ± 0.9	3.90 ± 0.32

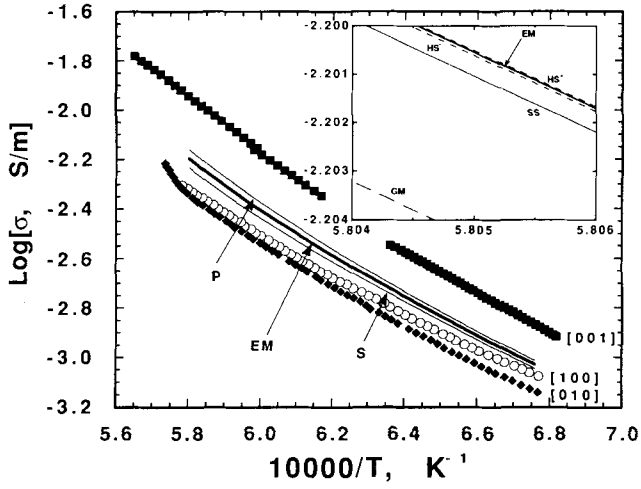

Figure 3. Original measurements and their best fits for conductivities in the three principal directions of olivine near the QFM buffer are shown with data points. Inside these are the parallel and series curves σ_p and σ_s. The magnified inset shows that $\sigma^{\pm}_{MW}$ [$= \sigma^{\pm}_{HS}$] and σ^{*}_{EM} [= SO1] fall virtually on the same line, but σ^{*}_{GM} and σ^{*}_{SS} are noticeably outside the HS bounds.

enough for most practical purposes, i.e., well within uncertainties of field data and of most laboratory measurements (Duba 1976; Haak 1982).

It is possible to use the three principal conductivities to obtain single conductivity values. The simplest method is the geometric mean formula

$$\sigma^*_{GM} = (\sigma_a \sigma_b \sigma_c)^{1/3} \tag{2}$$

which is plotted in Fig. 3.

Although (2) lacks theoretical justification, Schulgasser (1977) has shown that it is possible to construct statistically homogeneous, isotropic (but not necessarily realistic) models that satisfy (2).

Another possibility, which is introduced here, is an iterative or self-similar solution σ^*_{ss} of the parallel and series formulae; the next step beyond (1) is to repeat the process:

$$\sigma_{p2} = (\sigma_p + \sigma_s)/2, \tag{3a}$$

$$\sigma_{s2}^{-1} = (\sigma_p^{-1} + \sigma_s^{-1})/2. \tag{3b}$$

Note that (3a) is the Voight–Reuss–Hill or VRH average (e.g., Watt, Davies & O'Connell 1976); we see from the existence of a series formula (3b) that the VRH average is actually biased toward high conductivities. Yet another reason for not using a VRH average is that cited by Watt *et al.* (1976) for the elasticity problem, that the VRH average can be far outside the Hashin–Shtrikman bounds given below. A better average comes from calculating σ_{pn} and σ_{sn} iteratively from the previous values for the $(n-1)$th case until σ_{pn} and σ_{sn} give the same value of σ^*_{SS} to some arbitrary precision. For these data σ_{p5} and σ_{s5} agree to one part in 10^8 at 1394 °C; σ^*_{SS} is plotted in Fig. 3.

With less theoretical support it is possible to use the two series and parallel bounds as starting values and then to obtain other limits using well-established two-component treatments in order to demonstrate their essential agreement. The Maxwell (1892) bounds derived for isolated conducting spheres in a conducting matrix and Waff's (1974) space-filling spherical shells are both self-consistent formulations with the same algebraic form

$$\sigma^{\pm}_{MW} = (\sigma_2 + 2f_2\sigma_2 + 2f_1\sigma_1)/(2 + f_1\sigma_2/\sigma_1 + f_1). \tag{4}$$

Here f_1 and f_2 are volume fractions of materials 1 and 2, and σ^+_{MW} is the upper bound in the case that $\sigma_1 > \sigma_2$; the lower bound σ^-_{MW} is obtained by interchanging the subscripts 1 and 2 in (4). The Hashin–Shtrikman (1962) bounds, said to be the narrowest restrictions on a two-phase composite in the absence of geometrical information, are

$$\sigma^{\pm}_{HS} = \sigma_1 + f_2[(\sigma_2 - \sigma_1)^{-1} + f_1/3\sigma_1]^{-1}. \tag{5}$$

Again, $\sigma_1 > \sigma_2$ and the lower bound is obtained by interchanging subscripts. Equations (4) are algebraically equivalent to (5). The curves for $\sigma^{\pm}_{MW}$ and $\sigma^{\pm}_{HS}$ are plotted in Fig. 3 using $\sigma_1 = \sigma_p$ and $\sigma_2 = \sigma_s$ for equal volume fractions $f_1 = f_2 = 0.5$. Because σ_p and σ_s differ by only 15 per cent, the upper and lower bounds derived from them are virtually identical, agreeing to four significant figures. It is worth remarking that σ^*_{SS}, σ^*_{GM}, and a second geometric mean formulation $(\sigma_s\sigma_p)^{1/2}$, not illustrated, are all outside (below) the MW and HS bounds.

Landauer's (1952) effective medium theory, which was earlier derived by Bruggeman (1935) for binary mixtures, is

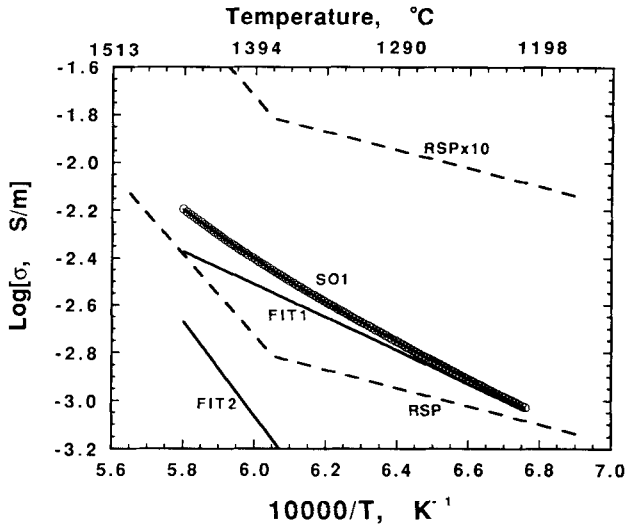

Figure 4. The best-fitting curve $\sigma^*_{EM} = SO1$ for the effective medium formulation together with the two exponential fits into which it is decomposed. Also shown are the curves RSP measured along [010] (Duba *et al.* 1974; adapted by Shankland & Waff 1977) and RSP×10.

a self-consistent scheme whose results lie between the MW and HS bounds. It is given by

$$\sigma^*_{EM} = 1/4\{(3f_1 - 1)\sigma_1 + (3f_2 - 1)\sigma_2 + [\langle(3f_1 - 1)\sigma_1 + (3f_2 - 1)\sigma_2\rangle^2 + 8\sigma_1\sigma_2]^{1/2}\}. \tag{6}$$

Figs 3 and 4 depict this result for $\sigma_1 = \sigma_p$, $\sigma_2 = \sigma_s$, and $f_1 = f_2 = 0.5$. This curve has been fitted to the sum of two exponentials in $1/T$ as described above and the results tabulated in Table 1. The numerical formula for σ^*_{EM} in S m^{-1} is

$$\sigma = 46.9e^{-1.38/kT} + 5.22 \times 10^8 e^{-3.90/kT}. \tag{7}$$

This result for an isotropic, homogeneous standard olivine, called SO1, improves upon the power-law formulation given by Shankland & Duba (1987) by fitting the data better and by permitting modest extrapolation beyond the temperature range of the data.

Fig. 4 also shows the curve RSP modified by Shankland & Waff (1977) from measurements of conductivity along [010] by Duba *et al.* (1974). In the modification, the two straight-line segments lie slightly above the equilibrium value of conductivity of RSP before partial melting, which occurred at about 1500 °C (Schock *et al.* 1989). Because RSP is lower than SO1, it can be seen that for a given conductivity, temperatures inferred from RSP would be higher than those from SO1.

4 UNCERTAINTIES IN CALCULATION OF GEOTHERMS

In the absence of textural information the effective medium formulation provides the most appropriate standard olivine curve for considering mantle conductivity. In using (7) to infer upper mantle temperatures the smallest uncertainties arise from experimental errors in temperature and oxygen fugacity. However, not knowing actual fO_2 in the mantle produces a worse uncertainty. We can use the variation of

conductivity as a function of oxygen fugacity at 1200 °C (Shock *et al.* 1989) to estimate this effect. Extrapolating the data to the edges of the stability field of olivine (as determined by Nitsan 1974) indicates that σ can vary as much as ±0.6 orders of magnitude from the average value determined at the midpoint of the olivine stability field. However, this worst case is not likely to be realized. Within the range of intrinsic oxygen fugacity determination reported for the mantle (Arculus & Delano 1981; Eggler 1983), the variation of conductivity is +0.2 to −0.4 log units [i.e., from wüstite-iron (WI) to QFM]. This variation translates to a temperature uncertainty at 1200° of +125°, −65 °C and at 1400° of +115°, −65 °C for the average conductivity SO1 determined here.

Only the worst-case uncertainties arising from the averaging procedures are larger than those from experimental uncertainties, but they are still not serious. At constant conductivity near 1400 °C, σ_p and σ_s produce a difference of 16 °C (or ±8°) in inferred temperature. These uncertainties are probably less than those associated with ignoring other phases or grain boundaries.

Worse uncertainties arise from uncertainties in mantle conductivities determined in the field. For instance, near 1400 °C a factor of two in conductivity (0.3 in log units) is equivalent to a variation of -0.30×10^{-4} to $+0.325 \times 10^{-4}$ in $1/T$ or +87° and −85 °C in temperature.

Grain boundaries and iron content have demonstrable effects in increasing conductivities (Haak 1982; Kariya & Shankland 1983), and for this reason Shankland & Waff (1977) tested a hypothetical upper bound RSP×10, also shown in Fig. 4. However, measurements by Constable & Duba (1990) on Jackson County dunite (JCD) having characteristic grain sizes of the order of 1 mm, which are more like the grain sizes of mantle xenoliths, fall about 1/2 order of magnitude below SO1 at 1200 °C. In this case where grain sizes are much larger than the fine-grained materials considered by Kariya & Shankland (1983) there appears to be little or no significant grain-boundary conductivity enhancement. Using the observation that olivine conductivity appears to increase with $x = [Fe/(Mg + Fe)]$ as $x^{1.8}$ (modified from Hirsch, Shankland & Duba 1989) and that olivine in JCD has $x = 0.073$, we can correct the JCD conductivity to the value $x = 0.093$ of this San Carlos olivine. This correction raises JCD conductivity by $0.19 \log_{10}$ units to within about 0.3 order of magnitude of SO1. Using JCD instead of SO1 would require a temperature about 85 °C higher in the region of 1200 °C to explain the same conductivity. Because JCD is not a direct sample of the mantle, SO1 probably is a more adequate first approximation of a mantle material.

It is not really possible to estimate uncertainties caused by the high pressures characteristic of mantle conditions. However, the pressure effect on conductivity of olivine is small (Dvorak 1973; Duba *et al.* 1974), probably because there are two conduction mechanisms in olivine whose pressure effects oppose each other (Schock *et al.* 1989).

5 CONCLUSIONS

The purpose of this paper has been to use the conductivity tensor of olivine to calculate an isotropic conductivity–temperature relationship and thus obtain a form suitable for inferring temperatures in the upper mantle. Under mantle conditions one expects olivine to be mixed with other minerals, most notably pyroxene, which can have a somewhat lower conductivity (Duba *et al.* 1973). In a Swiss cheese analogy olivine is the cheese and other, more insulating phases comprise the holes. Possibly balancing this low-conductivity tendency is enhancement expected from the presence of grain boundaries (Haak 1982; Kariya & Shankland 1983). Thus we judge that, at any given temperature in the mantle, conductivities calculated from (7) would indeed be close to probable mantle conductivities; hence, temperatures calculated from (7) or Fig. 4 would be reasonable approximations. Any high σ phase such as partial melt, sulfide, or carbon that would raise bulk σ would produce a lower calculated T.

Note that because σ_a along [100] is an intermediate value close to that of the various averages, a preferred orientation along this direction as has been proposed to explain elastic anisotropy with respect to mid-ocean ridge structure (Forsyth 1975; Christensen & Salisbury 1979) should not have a drastic effect on inferred electrical conductivity. A spatially averaged curve such as SO1 should not differ detectably from this particular instance of anisotropy, at least within the presently attainable accuracy of electromagnetic methods.

Curve SO1 is preferred to models such as RSP or RSP×10 because it is a better approximation to a mantle whose conductivity is governed by a homogeneous distribution of olivine. This arises because SO1 represents the average of the conductivity tensor of mantle-derived olivine measured under controlled oxygen fugacity appropriate to the upper mantle.

ACKNOWLEDGMENTS

We thank E. A. Arnold for expert assistance in developing software for data collection and analysis, S. C. Constable for the suggestion of non-linear fitting to exponential curves, and J. M. Brown for an adaptation of the Levenberg–Marquardt routine. This work was supported by the Office of Basic Energy Sciences of the US Department of Energy under contract W-7405-ENG-48 at Lawrence Livermore National Laboratory and under contract W-7405-ENG-36 at Los Alamos National Laboratory.

REFERENCES

Arculus, R. J. & Delano, J. W., 1981. Intrinsic oxygen fugacity measurements; Techniques and results for spinels from upper mantle peridotites and megacryst assemblages, *Geochim. Cosmochim. Acta*, **45**, 899–913.

Bruggeman, D. A. G., 1935. Berechnung verschiedener physikalischer Konstanten von heterogen Substanzen. I. Dielectrizitätskonstanten und Leitfähigkeiten der Mischköper aus isotropen Substanzen, *Annalen d. Physik*, **24**, 636–679.

Christensen, N. I. & Salisbury, M. H., 1979. Seismic anisotropy in the oceanic upper mantle: Evidence from the Bay of Islands ophiolite, *J. geophys. Res.*, **84**, 4601–4610.

Constable, S. C. & Duba, A. G., 1990. The electrical conductivity of olivine, a dunite, and the mantle, *J. geophys. Res.*, **95**, 6967–6978.

Duba, A. G., 1976. Are laboratory electrical conductivity data

relevant to the earth? *Acta Geodaet. Geophys. et Montanist. Acad. Sci. Hung.*, **11,** 485–495.

Duba, A. G. & Nicholls, I. A., 1973. The influence of oxidation state on the electrical conductivity of olivine, *Earth planet. Sci. Lett.*, **18,** 59–64.

Duba, A. G. & Shankland, T. J., 1982. Free carbon and electrical conductivity in the earth's mantle, *Geophys. Res. Lett.*, **9,** 1271–1274.

Duba, A. G., Boland, J. N. & Ringwood, A. E., 1973. The electrical conductivity of pyroxene, *J. Geol.*, **81,** 727–735.

Duba, A. G., Heard, H. C. & Schock, R. N., 1974. Electrical conductivity of olivine at high pressure and under controlled oxygen fugacity, *J. geophys. Res.*, **79,** 1667–1673.

Duba, A. G., Young, M. & Shankland, T. J., 1988. Electrical conductivity of synthetic olivine to 1500°C, *EOS, Trans. Am. geophys. Un.*, **69,** 1368.

Dvorak, Z., 1973. Electrical conductivity of several samples of olivinites, peridotites, and dunites, as a function of pressure and temperature, *Geophysics*, **38,** 14–24.

Eggler, D. H., 1983. Upper mantle oxidation state: evidence from olivine–orthopyroxene–ilmenite assemblages, *Geophys. Res. Lett.*, **10,** 365–368.

Forsyth, D. W., 1975. The early structural evolution and anisotropy of the oceanic upper mantle, *Geophys. J. R. astr. Soc.*, **43,** 103–162.

Haak, V., 1982. A comparison of electrical conductivity of natural mono- and polycrystalline olivines—a case to decide, in *High-Pressure Researches in Geoscience*, pp. 407–417, ed. Schreyer, W., Schweizerbartsche Verlagsbuchhandlung, Stuttgart.

Hashin, Z. & Shtrikman, S., 1962. A variational approach to the theory of the effective magnetic permeability of multiphase materials, *J. appl. Phys.*, **33,** 3125–3131.

Hirsch, L. M., Shankland, T. J. & Duba, A. G., 1989. Electrical conductivity and mobility in olivine, *EOS, Trans. Am. geophys. Un.*, **70,** 1368.

Hughes, H., 1955. The pressure effect on the electrical conductivity of peridot, *J. geophys. Res.*, **60,** 187–191.

Kariya, K. A. & Shankland, T. J., 1983. Electrical conductivity of dry lower crustal rocks, *Geophysics*, **48,** 52–61.

Kohlstedt, D. L., Goetze, C., Durham, W. B. & Vander Sande, J. B., 1976. A new technique for decorating dislocations in olivine, *Science*, **191,** 1045–1046.

Landauer, R., 1952. The electrical resistance of binary metallic mixtures, *J. appl. Phys.*, **23,** 779–784.

Maxwell, J. C., 1892. *A Treatise on Electricity and Magnetism*, 3rd edn, vol. 1, chapter 9, Clarendon, Oxford.

Netherton, R. & Duba, A. G., 1978. An apparatus for simultaneously measuring electrical conductivity and oxygen fugacity, *Report UCRL-52394*, Lawrence Livermore National Laboratory, Livermore, California.

Nitsan, U., 1974. Stability field of olivine with respect to oxidation and reduction, *J. geophys. Res.*, **79,** 706–711.

Press, W. H., Flannery, B. P., Teukolsky, S. A. & Vetterling, W. T., 1986. *Numerical Recipes*, chapter 14, pp. 498–546, Cambridge University Press, Cambridge.

Reuss, A., 1929. Berechnung der Fliessgrense von Mischkristallen auf Grund der Plastizitätsbedingung für Einkristalle, *Zeitschrift f. angewandte Mathematik und Mechanik*, **9,** 49–58.

Runcorn, S. K. & Tozer, D. C., 1955. The electrical conductivity of olivine at high temperatures and pressures, *Ann. d. Geophysique*, **11,** 98–102.

Schock, R. N., Duba, A. G. & Shankland, T. J., 1989. Electrical conduction in olivine, *J. geophys. Res.*, **94,** 5829–5839.

Schulgasser, K., 1976. Relationship between single-crystal and polycrystal electrical conductivity, *J. appl. Phys.*, **47,** 1880–1886.

Schulgasser, K., 1977. Bounds on the conductivity of statistically isotropic polycrystals, *J. Phys. C: Sol. State. Phys.*, **10,** 407–417.

Shankland, T. J. & Waff, H. S., 1977. Partial melting and electrical conductivity anomalies in the upper mantle, *J. geophys. Res.*, **82,** 5409–5417.

Shankland, T. J. & Duba, A. G., 1987. Spatially averaged electrical conductivity curve for olivine, *EOS, Trans. Am. geophys. Un.*, **68,** 1503.

Shankland, T. J., O'Connell, R. J. & Waff, H. S., 1981. Geophysical constraints on partial melt in the upper mantle, *Revs. Geophys. Space Phys.*, **19,** 394–406.

Tozer, D. C., 1959. The interpretation of upper-mantle electrical conductivities, *Tectonophysics*, **56,** 147–163.

Voight, W., 1928. *Lehrbuch der Kristallphysik*, Teuber, Leipzig.

Waff, H. S., 1974. Theoretical considerations of electrical conductivity in a partially molten mantle and implications for geothermometry, *J. geophys. Res.*, **79,** 4003–4010.

Watt, J. P., Davies, G. F. & O'Connell, R. J., 1976. The elastic properties of composite materials, *Rev. Geophys. Space Phys.*, **14,** 541–563.